Iranian Journal of Numerical Analysis and Optimization
Vol. 11, No. 2, (2021), pp 485-511
DOI:10.22067/ijnao.2021.70940.1051

Research Article

Review of the strain-based formulation for analysis of plane structures

Part II: Evaluation of the numerical performance

M. Rezaiee-Pajand*, N. Gharaei-Moghaddam and M. Ramezani

Abstract

In this part of the study, several benchmark problems are solved to evaluate the performance of the existing strain-based membrane elements, which were reviewed in the first part. This numerical evaluation provides a basis for comparison between these elements. Detailed discussions are offered after each benchmark problem. Based on the attained results, it is concluded that inclusion of drilling degrees of freedom and also utilization of higher-order assumed strain field result in higher accuracy of the elements. Moreover, it is evident that imposing the optimal criteria such as equilibrium and compatibility on the assumed strain field, in addition to reducing the number of degrees of freedom of the element, increases the convergence speed of the resulting strain-based finite elements.

AMS subject classifications (2020): 74K15, 74G15.

Keywords: Strain-based formulation; Higher-order strain field; Equilibrium condition; Numerical evaluation; Drilling degrees of freedom.

---

*Corresponding author
Received 25 October 2020; revised 8 June 2021; accepted 9 June 2021
Mohammad Rezaiee-Pajand
Professor of Civil Engineering, School of Engineering, Ferdowsi University of Mashhad, Iran. e-mail: Rezaiee@um.ac.ir, Tel/fax: +98-51-38412912

Nima Gharaei-Moghaddam
PhD of Structural Engineering, School of Engineering, Ferdowsi University of Mashhad, Iran. e-mail: Nima.Gharaei@gmail.com, Tel: +98-915-1589342

Mohammadreza Ramezani
PhD Student of Structural Engineering, School of Engineering, Ferdowsi University of Mashhad, Iran. e-mail: Mohammadrezaramezani1994@gmail.com, Tel: +98-915-1076010

1 Introducton

Among different formulation methods for the development of membrane finite elements, the assumed strain approach is proved to be very effective in removing problems such as shear parasitic error, mesh sensitivity, and different locking phenomena [28]. Therefore, various authors utilized this scheme to develop strain-based plane elements [6]. These finite elements were reviewed in the first part of this study. The main objective of the second part is to evaluate the numerical performance of the reviewed elements and study the effect of different assumptions and criteria on the performance of assumed strain formulation. For this purpose, the results attained by the reviewed elements for a series of benchmark problems are presented. Based on the obtained results by the reviewed membrane elements, a short discussion is provided after each problem. Moreover, according to the overall outcomes, the existing strain-based plane elements are ranked according to their different advantages and shortcomings. This ranking can be used to detect the most suitable assumptions and configurations to achieve a robust plane finite element. It should be noted that in the present paper, only the performance of the strain-based membrane elements in the analysis of linear problems is investigated. This is mainly because even the finite elements developed for nonlinear applications first should pass the upcoming benchmark tests to be considered as robust and powerful elements. It is also reminded that most of the reviewed research works evaluated the performance of their suggested elements in the analysis of linear problems. However, it is obvious that the reviewed element can also be used for the analysis of nonlinear problems and some of the previously published pursued this issue. The interested readers can refer to references [14, 26] for further information in this regard.

Tables 1 and 2 present a list of the elements used for comparison.

As it can be seen, an abbreviation is used for each element, which is selected based on the following order. The first part of the abbreviation is taken from the authors' names. The second part of the abbreviation starts with a letter that indicates the geometric shape of the element. Accordingly, "T", "Q", and "R" stand for triangular, quadrilateral, and rectangular, respectively. This letter is followed by a number that indicates the number of degrees of freedom. If the drilling degrees of freedom are used in the formulation of an element, then the letter "D" comes after the previously mentioned number. Finally, if two or more elements with the same geometry and number of nodes are proposed by the same authors, then roman numerals distinct those elements. For instance, based on this abbreviation method, the triangular element proposed by Belarbi and Bourezane, which has nine degrees of freedom and includes drilling degrees of freedom is called "BB-T9D", and since two different elements with the same abbreviation in this convention exist, they are distinguished from each other by roman numerals as "BB-T9D-I" and "BB-T9D-II".

Table 1: List of triangular plane elements used for comparison

No.	Abbreviation	Description of the element	Reference
		Triangular Elements	
1	S-T9D	Three-node nine-degree of freedom triangular element with drilling proposed by Sabir	[28]
2	SS-T8	Four-node eight-degree of freedom triangular element proposed by Sabir and Sfendji	[29]
3	T-T9D	Three-node nine-degree- of freedom triangular element with drilling proposed by Tayeh	[30]
4	BB-T9D-I	First three-node nine-degree of freedom triangular element with drilling proposed by Belarbi and Bourezane	[2]
5	BB-T9D-II	Second three-node nine-degree of freedom triangular element with drilling proposed by Belarbi and Bourezane	[3]
6	RY-T10	Six-node ten-degree of freedom triangular element proposed by Rezaiee-Pajand and Yaghoobi	[25]
7	RY-T10D	Seven-node ten-degree of freedom triangular element with drilling proposed by Rezaiee-Pajand and Yaghoobi	[26]
8	R-T9D	Three-node nine-degree of freedom triangular element with drilling proposed by Rebiai	[13]
9	RGR-T10	Five-node ten-degree of freedom triangular element proposed by Rezaiee-Pajand et al.	[17]
10	RGR-T10D	Four-node ten-degree of freedom triangular element with drilling proposed by Rezaiee-Pajand et al.	[17]
11	RGR-T11D-I	Seven-node eleven-degree of freedom triangular element with drilling proposed by Rezaiee-Pajand et al.	[18]
12	RGR-T11D-II	Four-node eleven-degree of freedom triangular element with drilling proposed by Rezaiee-Pajand et al.	[19]
13	RGR-T14	Seven-node fourteen-degree of freedom triangular element proposed by Rezaiee-Pajand et al.	[22]

In addition to the reviewed membrane elements, which are formulated by the assumed strain approach, results of three common displacement-based elements namely four-node and eight-node isoparametric quadrilateral elements (Q4 and Q8) and linear strain triangular element (LST) are provided in some problems to compare the performance of the strain-based formulation with them.

Table 2: List of quadrilateral plane elements used for comparison

No.	Abbreviation	Description of the element	Reference
		Quadrilateral Elements	
1	SS-R10	Five-node ten-degree of freedom rectangular element proposed by Sabir and Sfendji	[29]
2	T-R12D	Four-node twelve-degree of freedom rectangular element with drilling proposed by Tayeh	[30]
3	BM-R10	Five-node ten-degree of freedom rectangular element proposed by Belarbi and Maalem	[4]
4	RY-Q10	Five-node ten-degree of freedom quadrilateral element proposed by Rezaiee-Pajand and Yaghoobi	[23]
5	RY-R10-I	First five-node ten-degree of freedom rectangular element proposed by Rezaiee-Pajand and Yaghoobi	[24]
6	RY-R10-II	Second five-node ten-degree of freedom rectangular element proposed by Rezaiee-Pajand and Yaghoobi	[24]
7	RB-R12D	Four-node twelve-degree of freedom rectangular element with drilling proposed by Rebiai and Belounar	[14]
8	RB-Q12D	Four-node twelve-degree of freedom quadrilateral element with drilling proposed by Rebiai and Belounar	[15]
9	RSB-Q12D	Four-node twelve-degree of freedom quadrilateral element with drilling proposed by Rebiai et al.	[16]
10	RY-Q14D	Five-node fourteen-degree of freedom quadrilateral element with drilling proposed by Rezaiee-Pajand and Yaghoobi	[27]
11	RY-Q18	Nine-node eighteen-degree of freedom quadrilateral element proposed by Rezaiee-Pajand and Yaghoobi	[8]

2 Numerical evaluation

In this section, several benchmark problems are solved to evaluate the performance of the strain-based elements, which were reviewed in the first part of this study. It should also be noted that in the following benchmark problems, consistent units are used for various quantities. Accordingly, the problems are presented in a dimensionless format. Moreover, it should be noted that except for the elements proposed by the authors themselves, the results of the other elements are taken from the related references, and many of the reviewed references did not report the results for some of the following problem. Therefore, in some problems, the results of some elements are not reported.

2.1 Cantilever beam with distorted mesh

One of the available tests to examine the performance of the membrane elements in the coarse distorted meshes, under both bending and shear loadings, is the cantilever beam, which is depicted in Figure 1 [6, 26].

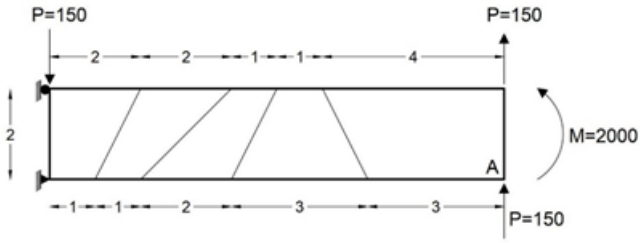

Figure 1: Cantilever beam with distorted quadrilateral mesh

This figure illustrates the geometric characteristics, loading, and utilized meshes for quadrilateral elements. The modulus of elasticity and Poisson's ratio of this beam are 1500 and 0.25, respectively, and its thickness is equal to 1. The utilized mesh for analysis using triangular elements is demonstrated in Figure 2. As it is evident, each quadrilateral element is divided by a dashed line into two triangular elements.

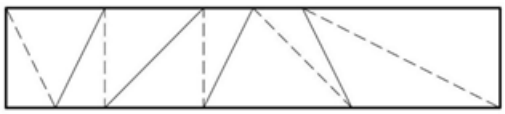

Figure 2: Triangular mesh for analysis Cantilever beam with distorted mesh

The analytical vertical displacements at point A under the shear and bending loadings are equal to 102.60 and 100, respectively. The attained results by Q4, Q8, and other strain-based elements are listed in Table 3. In fact, this test measures the performance of different elements for the analysis of structures with distorted meshes under bending and shear loading conditions. According to the results, almost all the strain-based elements, except T-T9D, provide acceptable accuracy. The most accurate quadrilateral element is RY-Q10 and BM-R10. Among the triangular elements, RGR-T10D, RGR-T11D-I, and RGR-T11D-II show the highest accuracy. An interesting finding is that, in general, the accuracy of the strain-based elements under flexural loading is higher. However, there are exceptions such as RY-Q18. Another important finding is the unexpectedly poor performance of T-T9D, which is the second weakest element after Q4. The attained results by RGR-T10 and RGR-T10D, which have the same assumed strain field and their differences are only in distribution and type of degrees of freedom, verify this

conjecture that inclusion of drilling degrees of freedom in the plane elements, improves their accuracy under in-plane bending.

Table 3: Deflection of point A of the cantilever beam with distorted mesh

	Element	Load P		Load M	
		Displacement	Relative Error (%)	Displacement	Relative Error (%)
Quadrilateral elements	Q4	50.70	50.58	45.70	54.30
	Q8	101.50	1.07	99.70	0.30
	SS-R10	97.91	4.51	98.57	1.43
	T-R12D	93.28	9.08	96.11	3.89
	BM-R10	101.77	0.81	99.93	0.07
	RY-Q10	102.79	0.18	100.00	0.00
	RB-R12D	98.83	3.67	97.30	2.70
	RB-Q12D	99.35	3.17	99.19	0.81
	RY-Q14D	104.16	1.52	101.66	1.66
	RY-Q18	103.52	0.89	101.48	1.48
Triangular elements	LST	101.05	1.51	98.30	1.70
	S-T9D	100.08	2.45	97.82	2.18
	SS-T8	100.89	1.67	98.36	1.64
	T-T9D	79.87	22.15	83.05	16.95
	RY-T10D	100.58	1.96	100.00	0.00
	R-T9D	100.98	1.57	99.86	0.14
	RGR-T10	103.65	1.02	98.50	1.50
	RGR-T10D	101.83	0.75	100.00	0.00
	RGR-T11D_I	103.92	1.29	100.70	0.70
	RGR-T11D_II	101.58	0.99	100.99	0.99
	RGR-T14	103.72	1.09	101.03	1.03
Analytical Solution		102.60	-	100.00	-

2.2 Cantilever beam under parabolic shear loading

To investigate the performance of the elements in the analysis of structures under distributed surface traction, the cantilever beam demonstrated in Figure 3 is analyzed [5, 12, 26].

This beam is made of an elastic material with the modulus of elasticity and Poisson's ratio equal to 3000 and 0.25, respectively and its thickness is taken one unit. The beam is loaded by the parabolic distributed traction at its free end, which is equal to 40 units. This benchmark problem also evaluates the efficiency of elements in the analysis of structures using coarse meshes. As it is evident in Figure 3, the beam is discretized by four quadrilateral elements.

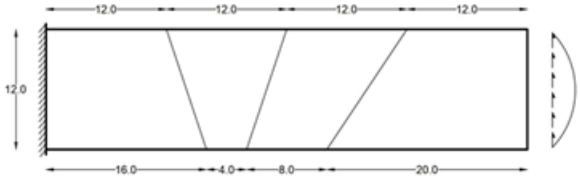

Figure 3: Cantilever beam under parabolic shear loading

In the case of triangular elements, eight elements are used, which the utilized mesh is demonstrated in Figure 4. However, results of some of the reviewed elements are reported for the regular mesh.

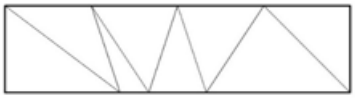

Figure 4: Triangular mesh for analysis Cantilever beam under parabolic shear loading

Table 4 presents the obtained responses by the mentioned membrane elements for deflections at the tip of the beam. Felippa reported the near-exact tip deflection of the beam equal to 0.35601 [7].

Based on the reported results, RGR-T10 and RY-Q14D are the most accurate elements in this problem with only 0.03 percent error in their estimations. Similar to the previous problem, T-T9D has the worst performance with 25 percent error, and again the RY-Q10 is among the most accurate quadrilateral elements. As it can be seen, RGR-T14 is among the most accurate elements. This was expected, since as mentioned in the respective reference, an important feature of the complete second-order assumed strain-filed is its ability in providing accurate responses for the problems with distributed loading [22].

2.3 Cook's skew beam

Cook trapezoidal beam is one of the most fundamental tests for checking shear displacements in non-rectangular geometry [6]. Figure 5 demonstrates this beam under uniformly distributed tip loading. This beam has a unit thickness and is made of a material whose Young's modulus and Poisson's ratio are 1 and $\frac{1}{3}$, respectively.

Many researchers also implement this benchmark to challenge the convergence of their elements. Here, four different meshes, namely 2×2, 4×4, 8×8, and 16×16, are used. These meshes are demonstrated in Figure 6. The

Table 4: Tip deflection of cantilever beam under parabolic shear

	Element	Vertical Displacement	Relative Error (%)
Quadrilateral elements	Q4	0.21290	40.20
	Q8	0.34790	2.28
	SS-R10	0.34070*	4.30
	T-R12D	0.31328	12.00
	BM-R10	0.34604*	2.80
	RY-Q10	0.35280	0.90
	RY-R10-I	0.32724*	8.08
	RY-R10-II	0.33027*	7.23
	RB-R12D	0.34120*	4.16
	RSB-Q12D	0.33470*	5.99
	RY-Q14D	0.35590	0.03
	RY-Q18	0.35230	1.04
Triangular elements	LST	0.34770	2.33
	T-T9D	0.26701	25.00
	BB-T9D-I	0.27822*	21.85
	RY-T10	0.35031*	1.60
	RY-T10D	0.34680	2.59
	RGR-T10	0.35610	0.03
	RGR-T10D	0.34680	2.59
	RGR-T11D-I	0.35850	0.70
	RGR-T11D-II	0.35713	0.31
	RGR-T14	0.35555	0.13
Near-exact solution		0.35601	

* The results are attained from a regular mesh

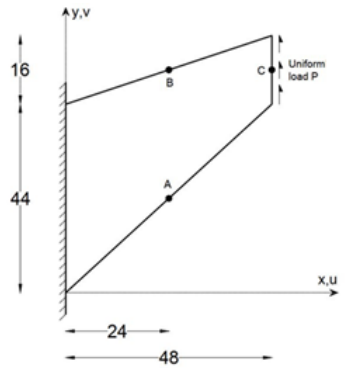

Figure 5: Cook's skew beam

results of the point C deflection are presented in Table 5. It should be noted that the near-exact solution for this problem is reported equal to 23.96 [21].

Outcomes of this problem are again in complete agreement with the findings of previous numerical examples, and once more, the RGR-T11D-I and RGR-T11D-II are among the best-performing elements. The other elements, which provide accurate estimations, are RY-Q10, RGR-T10, and R-T9D. It is somehow unexpected that R-T9D can compute a very accurate response by a coarse 4×4 mesh. One of the elements that have relatively fast convergence is RGR-T14. As it is evident, the convergence trend of different elements is not similar. While most of the elements converge to the exact response asymptotically from below, the RGR-T11D-I element approaches the accurate response from above. Also, there are elements, such as RY-T10 and RY-T10D, which show non-uniform convergence behavior, and even RY-Q14D goes beyond the response. Nevertheless, most of the strain-based elements demonstrate reasonable accuracy and convergence in this benchmark problem.

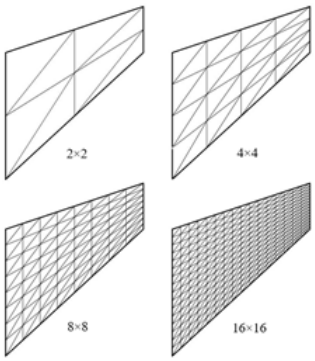

Figure 6: Utilized meshes for analysis of Cook's skew beam

2.4 Thick curved beam

To appraise the ability of finite elements, especially triangular ones, in the analysis of structures with curved geometry, many of the previous researchers have evaluated the performance of their proposed element in solving the curved beams, which is demonstrated in Figure 7 [5, 26, 32]. This beam is loaded by the shear load $P = 600$ at its tip.

The module of elasticity, poison's ratio, and thickness of this beam are 1000, 0, and 1, respectively. As depicted in Figure 7, four quadrilateral elements are used to mesh this structure. In the case of triangular elements, eight elements are used as demonstrated in Figure 8.

Table 5: Deflection of point C of the Cook's beam

		Mesh			
	Element	2×2	4×4	8×8	16×16
Quadrilateral elements	Q4	11.80	18.29	22.08	23.43
	SS-R10	17.06	30.64	30.64	30.65
	T-R12D	14.85	17.25	19.88	21.80
	RY-Q10	25.65	24.27	24.01	23.96
	RB-Q12D	17.87	23.37	23.38	23.50
	RY-Q14D	27.61	30.48	31.85	32.44
	RY-Q18	23.45	23.70	23.86	23.92
Triangular elements	S-T9D	18.25	20.32	22.18	22.18
	SS-T8	17.86	20.15	21.21	21.46
	T-T9D	12.45	15.09	18.44	20.13
	BB-T9D-I	18.52	21.36	22.45	23.69
	BB-T9D-II	18.58	23.88	23.88	23.88
	RY-T10	20.94	23.84	24.18	24.13
	RY-T10D	25.82	27.19	27.23	27.09
	R-T9D	18.78	23.94	23.94	23.94
	RGR-T10	21.18	23.03	23.69	23.95
	RGR-T10D	19.06	22.85	23.14	23.87
	RGR-T11D-I	26.00	24.39	24.01	23.97
	RGR-T11D-II	23.37	23.42	23.93	23.97
	RGR-T14	23.64	23.73	23.85	23.96
Near-exact Solution		23.96			

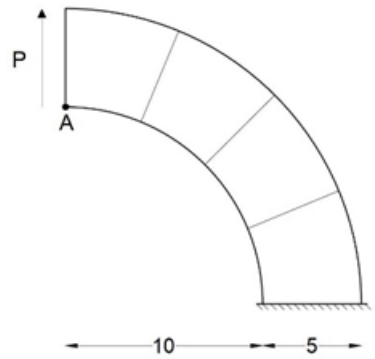

Figure 7: Thick curved beam with quadrilateral mesh

The exact vertical displacement of point A under the applied load is equal to 90.10. The attained results by different elements are presented in Table

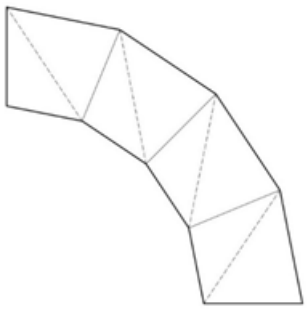

Figure 8: The triangular mesh for analysis of thick curved beam

6. It is evident that the RGR-T11D-I element provides the most accurate estimation with only 0.24% error. After this element, RGR-T10 with the relative error of 0.79% is in the second place. It is interesting to note that among the quadrilateral elements, the performance of Q8 is better than the strain-based elements. Nonetheless, the error of most of the strain-based elements is less than 5 percent, which for the utilized coarse mesh is negligible by any set of standards. This problem shows that the elements formulated by the assumed strain approach are a suitable option for efficient analysis of curved structures, and can compete with isoparametric elements in terms of accuracy and convergence.

Table 6: Deflection of point A of thick curved beam

	Element	Load P	
		Vertical Displacement	Relative Error (%)
Quadrilateral elements	Q8	88.60	1.66
	SS-R10	98.71	9.56
	RY-Q10	86.92	3.53
	RY-Q14D	87.00	3.44
	RY-Q18	86.45	4.05
Triangular elements	RY-T10	87.15	3.27
	RY-T10D	87.47	2.92
	RGR-T10	89.39	0.79
	RGR-T10D	84.62	6.08
	RGR-T11D-I	89.88	0.24
	RGR-T11D-II	88.30	2.00
	RGR-T14	83.79	7.00
Analytical Solution		90.10	

2.5 Thin curved beam

To investigate the effect of the shear lock-in curved structures and also the convergence rate to achieve the precise response, a thin curved beam test is available. The modulus of elasticity, Poisson's ratio, and thickness of this structure, which is demonstrated in Figure 9 are 10^7, 0.25, and 0.1, respectively [31, 32]. This beam is loaded by a unit vertical force at its tip.

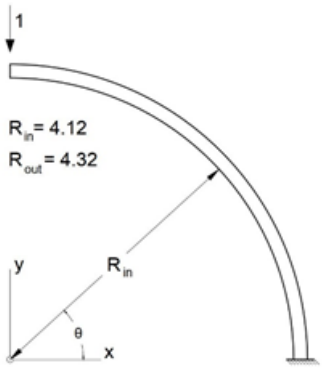

Figure 9: Thin curved beam

Three different meshes are used to analyze this structure, namely 1×6, 2×12, and 4×24. These meshes are named based on the number of quadrilateral elements used in them. Needless to say, for analysis using triangular elements, each quadrilateral element is divided into two triangular elements. For instance, 1×6 is demonstrated in Figure 10.

Figure 10: The used 1×6 mesh for analysis of thin curved beam

The main purpose of solving this problem is to compute the tip deflection of the beam under applied load and therefore, investigate the effect of the

locking problem on the performance of the strain-based elements. The exact vertical displacement at the tip is reported to be equal to 0.08734[23]. Table 7 presents the obtained results by some of the strain-based elements.

Table 7: Deflection of point A of thin curved beam

	Element	Mesh					
		1×6		2×12		4×24	
		Deflection	Relative Error (%)	Deflection	Relative Error (%)	Deflection	Relative Error (%)
Quadrilateral elements	RY-Q10	-0.08901	1.91	-0.08844	1.26	-0.08846	1.28
	RY-Q14D	-0.08748	0.16	-0.08898	1.87	-0.08925	2.19
	RY-Q18	-0.08745	0.12	-0.08840	1.21	-0.08850	1.33
Triangular elements	RY-T10	0.05634	35.49	0.08491	2.78	0.08815	0.93
	RGR-T10	-0.06305	27.81	-0.08493	2.76	-0.08609	1.43
	RGR-T10D	-0.06486	25.74	-0.08501	2.67	-0.08650	0.96
	RGR-T11D	-0.08291	5.07	-0.08434	3.43	-0.08691	0.49
	RGR-T11D	-0.08265	5.36	-0.08656	0.89	-0.08622	1.28
	RGR-T11D	-0.08712	0.25	-0.08713	0.24	-0.08728	0.07
Analytical Solution		-0.08734					

It is evident that the mentioned triangular elements, except the RGR-T11D-I and II and RGR-T14, face the locking problem in the coarsest mesh and behave too stiffly. In contrast, these elements provide an acceptable response. In the coarsest mesh, these elements do not lock and have a maximum error of 5.36%. This error reduces to 0.07% in the finest mesh. It should be noted that the quadrilateral elements provide more accurate estimations in the coarse mesh. However, in the case of the finest utilized mesh, they tend to become a bit more flexible and therefore, predict responses higher than the exact values.

2.6 McNeal's beam

McNeal and Harder proposed this benchmark to examine the sensitivity of the elements to the mesh distortion and the trapezoidal locking phenomenon [9]. The geometry of this beam and the rectangular, parallelogram, and trapezoidal meshes used for analysis by quadrilateral elements are depicted in Figure 11. The utilized meshes for triangular meshes are demonstrated in Figure 12.

Modulus of elasticity, Poisson's ratio, and thickness of the structure are 10^7, 0.3, and 0.1, respectively. Two modes of loading are assumed, as depicted in Figure 10. The derived responses by the strain-based elements are listed in Table 8. This test is a difficult problem for many of the displacement-based membrane elements since they demonstrate high sensitivity to the trapezoidal meshes. For example, the powerful Q8 element with all of its capabilities

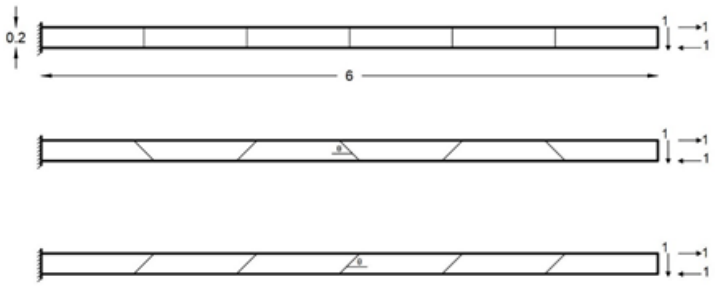

Figure 11: McNeal's beam and utilized quadrilateral meshes

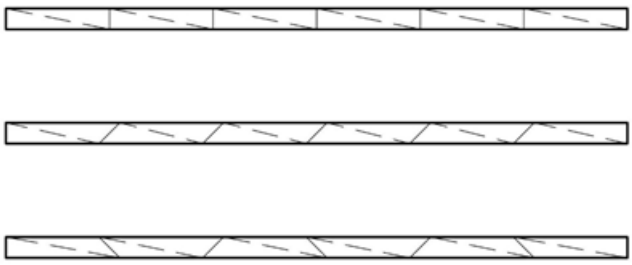

Figure 12: The utilized triangular meshes for analysis of McNeal's beam

faces fatal error for both modes of loading in trapezoidal mesh. However, as it is evident from the results presented in Table 7, most of the strain-based elements have no problem in this case. Although SS-R10 and S-T9D are exceptions, they suffer from trapezoidal locking severely. It is interesting to note that the RGR-T11D-II provides very accurate estimations for the shear loading without any problem due to locking, while most of the other elements face the trapezoidal locking under shear loading. In the flexural loading, RGR-T14 can capture the exact response in all the utilized meshes.

2.7 Higher-order patch test

The beam, which is demonstrated in Figure 13, is the next numerical example that evaluates the performance of plane strain-based elements.

This beam, which has a geometric ratio of 10, is made of the elastic material with a modulus of elasticity and Poisson's ratio equal to 100 and 0, respectively. The thickness of the beam is taken as 1. Two different types of meshes, namely regular and distorted, which are demonstrated in Figure 14, are used.

Table 8: Normalized tip deflection of the McNeal's beam

	Element	Load P			Load M		
		Rectangular mesh	Parallelogram mesh	Trapezoidal mesh	Rectangular mesh	Parallelogram mesh	Trapezoidal mesh
Quadrilateral elements	Q4	9.30	3.58	3.06	9.34	3.14	2.21
	Q8	95.12	91.94	85.43	100.00	75.94	9.32
	SS-R10	4.62	3.61	0.00	11.77	10.07	0.37
	RY-Q10	99.30	99.42	99.42	100.00	100.00	100.00
	RB-Q12D	99.26	98.69	98.78	99.63	99.26	99.26
	RSB-Q12D	100.00	97.59	97.78	100.00	98.89	98.89
	RY-Q14D	98.33	98.74	98.79	98.88	99.11	99.19
	RY-Q18	100.00	100.00	100.00	100.00	100.00	100.00
Triangular elements	LST	98.3	97.05	96.12	99.34	99.40	99.22
	S-T9D	4.75	3.63	0.05	11.82	10.13	0.04
	BB-T9D-I	94.42	87.40	83.35	94.83	94.42	95.21
	BB-T9D-II	96.40	95.04	98.82	98.94	98.79	98.81
	RY-T10	99.44	94.30	92.11	100.00	100.00	100.01
	RY-T10D	99.43	94.94	92.31	100.00	100.00	100.00
	R-T9D	99.63	97.87	97.87	99.62	99.25	99.25
	RGR-T10	99.41	99.52	99.92	100.00	99.95	100.00
	RGR-T10D	99.33	94.12	90.56	100.00	99.98	100.00
	RGR-T11D-I	104.34	102.48	104.99	100.79	100.56	100.94
	RGR-T11D-II	100.00	100.00	100.30	107.40	108.80	106.90
	RGR-T14	0.994	0.995	0.995	100.00	100.00	100.00
Analytical Solutions			0.1081			0.0054	

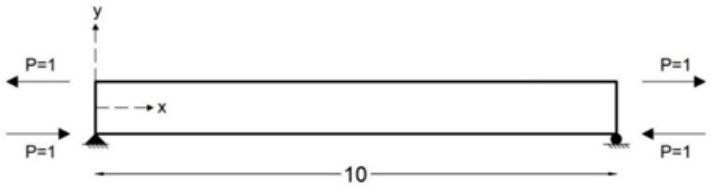

Figure 13: Higher-order patch test

This test examines the performance of the elements under pure bending and considering the simple support conditions. The attained results by the strain-based elements are listed in Table 9. It is evident that all of the elements can compute the exact response regardless of the utilized mesh.

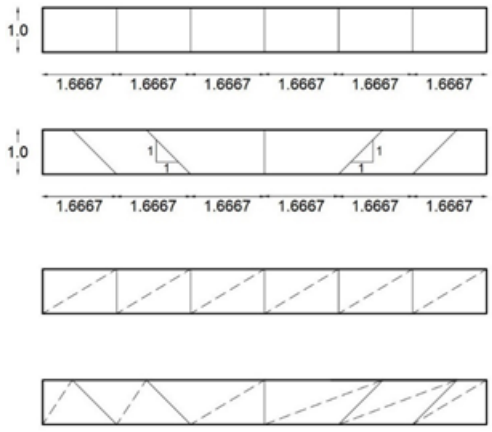

Figure 14: Utilized regular and distorted meshes

Table 9: Maximum displacements of the higher-order patch test

Element		Regular mesh		Distorted mesh	
		Max U	Max V	Max U	Max V
Quadrilateral elements	RY-Q10	-0.600	1.500	-0.600	1.500
	RY-R10-I	-0.600	1.500	-0.600	1.500
	RB-R12D	-0.600	1.500	-0.600	1.500
	RB-Q12D	-0.594	1.493	-0.592	1.484
	RSB-Q12D	-0.590	1.500	-0.590	1.490
	RY-Q14D	-0.600	1.500	-0.600	1.500
	RY-Q18	-0.600	1.500	-0.600	1.500
Triangular elements	RY-T10D	-0.600	1.500	-0.600	1.500
	RGR-T10	-0.600	1.500	-0.600	1.500
	RGR-T10D	-0.600	1.500	-0.600	1.500
	RGR-T11D-I	-0.600	1.500	-0.600	1.500
	RGR-T11D-II	-0.600	1.500	-0.600	1.500
	RGR-T14	-0.600	1.500	-0.600	1.500
Analytical Solution		-0.600	1.500	-0.600	1.500

2.8 Thick-walled cylinder

The cylindrical plane strain test of the thick wall under uniform internal pressure is the eighth problem, which investigates the effect of the Poisson's locking on the performance of strain-based elements [1]. Due to symmetry, only a quarter of this cylinder will be analyzed. This structure and utilized mesh are depicted in Figure 15.

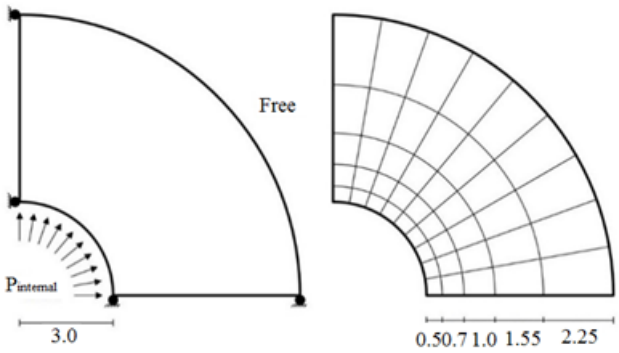

Figure 15: Thick-walled cylinder and used mesh

The elastic modulus of the material is 1000, and it is solved for different values of Poisson's ratio varying from 0.3 to 0.4999. The derived results by different elements are presented in Table 10. According to the outcomes, the assumed strain approach results in elements free from the Poisson's locking.

Table 10: Normalized radial displacement of the thick-walled cylinder at the inner radius

Element		Poisson's ratio			
		0.3	0.49	0.499	0.4999
Quadrilateral elements	RY-Q10	0.9799	0.9789	0.9790	0.9794
	RY-Q14D	1.1805	1.1839	1.1841	1.1846
	RY-Q18	0.9360	0.9576	0.9593	0.9599
Triangular elements	BB-T9D-I	0.9743	-	-	-
	RGR-T11D-I	1.01869	1.0356	1.0361	1.0365
	RGR-T11D-II	1.02838	1.04484	1.04545	1.04604
	RGR-T14	1.07564	1.07724	1.07726	1.07527
Analytical Solution [12]		0.00506	0.00506	0.00504	0.00458

2.9 Theoretical slender beam

The beam depicted in Figure 16, with a length of 100 is made of an elastic material with Young's modulus and Poisson's ratio of 10^6 and 0.3, respectively. This structure is used to investigate the shear effect on the slender plane problems. This structure is analyzed using two different meshes. The obtained results for tip displacements of the beam are listed in Table 11. RGR-T10 has the best performance among the reported elements. It is evi-

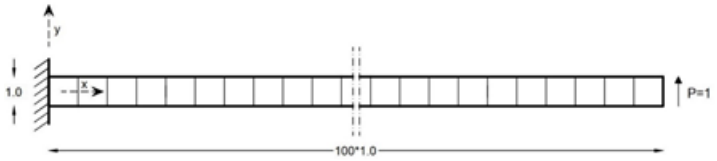

Figure 16: Extremely slender cantilever beam

dent that Q4 suffers from the locking problem and therefore, cannot compute the exact response even using a fine mesh.

Table 11: Tip displacements of slender cantilever beam

Element		Mesh	Displacements Ux ×100	Uy
Quadrilateral elements	Q4	1×100	2.0222	2.6965
		2×200	2.1280	2.8371
	RY-Q10	1×100	3.0046	4.0067
		2×200	2.9991	3.9982
	RY-R10-I	1×100	3.0046	4.0067
		2×200	2.9991	3.9982
	RY-R10-II	1×100	3.0000	4.0002
		2×200	2.9987	3.9976
	RY-Q14D	1×100	3.0000	4.0067
		2×200	3.193	4.2581
	RY-Q18	1×100	2.9983	3.9967
		2×200	2.9989	3.9980
Triangular elements	RY-T10	1×100	3.0000	4.0001
		2×200	2.9992	3.9986
	RGR-T10	1×100	3.0000	4.0000
		2×200	3.0000	4.0000
	RGR-T10D	1×100	2.9845	3.9767
		2×200	2.9944	3.9975
	RGR-T11D-I	1×100	3.0001	4.0003
		2×200	3.0001	4.0001
	RGR-T11D-II	1×100	3.0002	4.0002
		2×200	3.0001	4.0000
	RGR-T14	1×100	3.0012	4.0131
		2×200	3.0007	4.0043
Analytical Solution			3	4

2.10 Cantilever beam with distortion parameter

A distorted mesh is a finite element mesh that some of its elements deviate vastly from the equilateral triangle and symmetric quadrilateral shapes. To study the influence of the distortion on the behavior of the strain-based elements and prove their superiority in comparison with displacement-based elements, the beam showed in Figure 17 is analyzed by using two quadrilateral or four triangular elements [6].

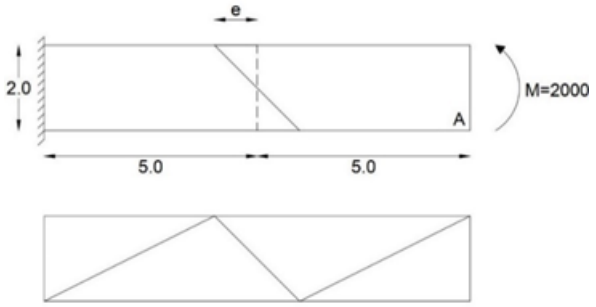

Figure 17: Cantilever beam with distortion parameter and utilized meshes

Table 12: Tip deflection of the cantilever beam with distortion parameter

Element		E						
		0	0.5	1	2	3	4	4.9
Quadrilateral elements	Q4	28.00	21.00	14.10	9.70	8.30	7.20	6.20
	Q8	100.00	99.90	99.30	89.39	59.70	32.01	-
	RY-Q10	100.00	100.00	100.00	100.00	100.00	100.00	100.00
	RY-Q14D	99.80	100.00	100.10	100.70	101.20	102.8	-
	RY-Q18	96.60	97.60	98.50	100.4	105.30	116.8	-
Triangular elements	S-T9D	45.08	45.33	45.84	47.96	49.15	49.47	-
	BB-T9D-I	96.02	96.60	97.04	97.40	97.26	96.90	-
	BB-T9D-II	96.02	96.60	97.04	97.40	97.26	96.90	-
	RY-T10D	100.00	100.00	100.00	100.00	100.00	100.00	100.00
	R-T9D	100.00	97.72	98.15	98.64	99.20	98.76	-
	RGR-T10	100.00	100.00	100.00	100.00	100.00	100.00	100.00
	RGR-T10D	100.00	100.00	100.00	100.00	100.00	100.00	100.00
	RGR-T11D-I	99.96	99.98	99.94	99.96	99.95	99.89	99.91
	RGR-T11D-II	100.00	100.00	100.00	100.00	99.95	99.91	99.89
	RGR-T14	100.00	100.00	100.00	100.00	104.90	114.70	114.73
Analytical Solution		100						

The beam is made of a material with a modulus of elasticity and Poisson's ratio equal to 1500 and 0.25, respectively and its thickness is taken equal to 1 unit. A distortion parameter, e, controls the shape of the elements. The thickness of the beam is taken equal to 1. This beam is reanalyzed by

increasing distortion parameter, and the attained results for tip deflection are listed in Table 12. As it can be seen, the strain-based elements are completely insensitive to the mesh distortion, and increasing the distortion parameter has no remarkable effect on their performance, while the accuracy of Q4 and Q8 diminishes rapidly by the increase in the distortion parameter. Another interesting finding of this numerical example is the poor performance of S-T9D, which is one of the first suggested strain-based elements.

2.11 Cantilever shear wall

An important purpose of formulating efficient elements is to analyze practical structures with coarser meshes and consequently fewer degrees of freedom. Therefore, in order to investigate the efficiency of the strain-based elements in practical problems, two shear walls are examined with the strain-based elements. In the first problem, the shear wall shown in Figure 18 is analyzed [24].

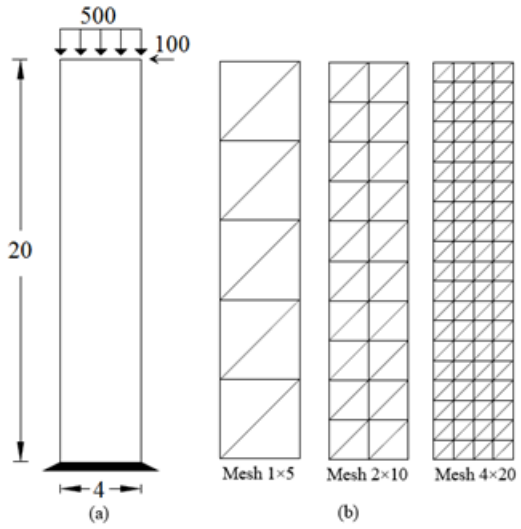

Figure 18: The shear wall and the utilized meshes

The modulus of elasticity and Poisson's ratio of the wall are 2×10^7 and 0.2, respectively. Here, to reevaluate the accuracy and efficiency of strain formulation, the conventional element Q8 is brought for comparison. Furthermore, to investigate the convergence, two finer meshes have been used. The normalized responses are provided in Table 13.

Based on the results presented in Table 13, the RGR-T14 element demonstrates the best performance among the compared elements. Two interesting

outcomes are the lower accuracy of Q8 and the inability of RY-Q14D, which becomes too flexible when using finer meshes. As it can be seen, all the reported strain-based elements except RGR-T10D have less than 5 percent error in their estimations when a coarse 1×5 meshes are used. Once again, this finding demonstrates the high efficiency of the assumed strain approach.

Table 13: Tip deflection of the cantilever beam with distortion parameter

Element		Mesh		
		1×5	2×10	4×20
Quadrilateral elements	Q8	62.17	80.10	89.17
	RY-R10-I	95.91	97.13	98.24
	RY-R10-II	95.87	96.99	98.19
	RY-Q14D	95.86	127.16	138.61
	RY-Q18	96.23	97.04	97.76
Triangular elements	RY-T10	96.86	97.53	98.35
	RGR-T10	96.62	97.78	98.12
	RGR-T10D	89.60	95.63	95.89
	RGR-T11D-I	96.21	98.56	99.01
	RGR-T11D-II	98.01	98.86	99.45
	RGR-T14	98.85	99.14	99.76
Near-exact solution			0.002570	

2.12 Coupled shear walls

In the last numerical example, two coupled shear walls are analyzed to study the performance of the elements in the presence of opening. This structure, which is demonstrated in Figure 19, is made of the elastic material with modulus of the elasticity and Poisson's ratio equal to 2×10^7 and 0.2, respectively [11].

The thickness of this structure is assumed 0.4. Lateral loads with an intensity of $P = 500$ are applied to each story level of the left shear wall. The structure is analyzed using two meshes consisting of 48 and 192 quadrilateral elements (96 and 384 triangular elements). To achieve a near-exact solution, the coupled wall is analyzed using 26880 eight-node isoparametric elements (Q8). The obtained results for lateral displacements at different story levels are reported in Table 14. It is evident that the RGR-T11D-II element provides the most accurate estimations. Based on the reported results for Q8 element, most of the strain-based membrane elements are more accurate and efficient. However, there is an exception about RY-Q14D, which becomes too flexible by using finer meshes and fails to converge to the exact response.

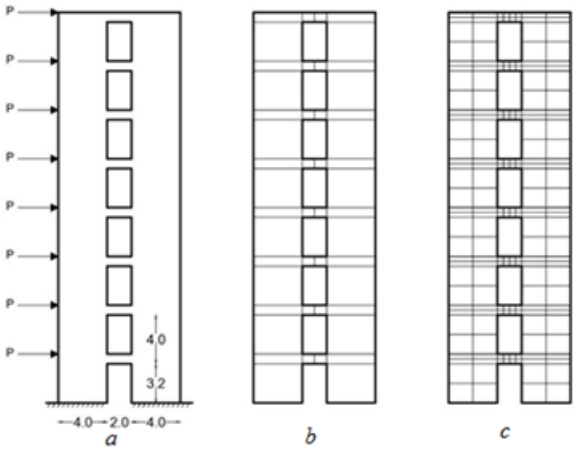

Figure 19: The Coupled shear wall and the utilized meshes a) applied lateral load b) coarse mesh with 48 elements c) fine mesh with 192 elements

3 Discussion

The performance of the existing strain-based plane elements reviewed in the first part of this study was evaluated using a series of benchmark problems in the previous section. First, a cantilever beam with distorted mesh was analyzed. The attained results showed low sensitivity of strain-based elements to mesh distortion compared to the classical displacement-based element, such as, Q4, Q8, and LST. Based on the reported results, the triangular elements are less sensitive than quadrilateral ones. In the next problem, the performance of the strain-based elements in the analysis of structures under distributed surface tractions with coarse mesh was evaluated. Once again, the superior performance of strain-based formulation in comparison with the displacement-based approach is demonstrated. It is also found that the higher-order elements provide better responses than others. However, the part of this better performance can be attributed to the larger number of degrees of freedom. To test the convergence trend of the elements, Cook's skew beam was analyzed using different plane elements. The derived results proved faster convergence of strain-based elements. However, their convergence trend is not uniform, that is, some elements converge to the exact solution form below and some other approaches the exact response from above.

The next two problems were devoted to assessing the performance of strain-based membrane elements in the analysis of structures with curved geometry. As it was expected, the triangular elements demonstrate better accuracy and faster convergence. It should be noted that some of the quadrilateral elements provided more accurate estimations than triangular ones in

Table 14: Lateral story displacements of the coupled shear wall

Element		Number of elements	Number of degrees-of-freedom	Lateral displacement Story 2	Story 4	Story 6	Story 8
Quadrilateral elements	Q8	48	440	0.56	1.53	2.59	3.64
		192	1348	0.68	1.82	3.02	4.16
	RY-R10-I	48	264	0.77	2.07	3.40	4.71
		192	844	0.78	2.07	3.44	4.71
	RY-R10-II	48	216	0.69	1.88	3.13	4.28
		192	668	0.74	2.00	3.32	4.65
	RY-Q14D	48	348	0.90	2.62	4.61	6.63
		192	962	1.14	3.22	5.49	7.70
	RY-Q18	48	540	0.76	2.03	3.36	4.61
		192	1700	0.80	2.13	3.51	4.81
Triangular elements	RY-T10	96	402	0.71	1.92	3.18	4.38
		384	1272	0.80	2.12	3.50	4.79
	RGR-T10	96	396	0.76	2.03	3.29	4.54
		384	1252	0.85	2.26	3.63	4.96
	RGR-T10D	96	348	0.73	1.94	3.19	4.45
		384	1018	0.82	2.14	3.55	4.86
	RGR-T11D-I	96	530	0.75	2.07	3.26	4.63
		384	1800	0.83	2.25	3.56	5.02
	RGR-T11D-II	96	444	0.78	2.15	3.35	4.66
		384	1442	0.88	2.31	3.67	5.19
	RGR-T14	96	732	0.69	1.96	3.05	4.18
		384	2404	0.85	2.21	3.48	4.99
Near-exact solution				0.90	2.38	3.91	5.35

the coarse mesh. However, in the case of the finest utilized mesh, they tend to become a bit more flexible and therefore, predict responses higher than the exact values. To show the insensitivity of the strain-based formulation to trapezoidal locking, the McNeal's beam was analyzed. In fact, the trapezoidal locking is generally a problem for quadrilateral displacement-based elements, such as, Q4 and Q8. Once more, utilization of strain-based quadrilateral elements removes this problem and results in highly accurate responses irrespective of the mesh type. Another problem, which tested the performance of the strain-based elements with respect to mesh distortion was the higher-order patch test. The results of this numerical test proved considerable the insensitivity of the strain-based element to mesh distortion. The effect of distortion extent on the accuracy of the element responses was also investigated in the tenth studied problem. In this part, a cantilever beam loaded with a bending moment at its free end was reanalyzed considering different distorted meshes. Based on the attained results, elements, such as, RY-Q10, RY-T10D,

RGR-T10, and RGR-T10D are completely insensitive to the mesh distortion irrespective of its extent. The other element, however, showed some deviation from the exact responses by introducing severe mesh distortion.

Another problem that occurs for the classical plane elements is the Poisson's locking phenomenon, in which the finite elements face difficulty in predicting accurate responses for the structures made of nearly incompressible material. Solving a thick-walled cylinder under internal pressure for different values of Poisson's ratio, it is shown that higher-order strain-based elements are free from this locking phenomenon. To assess the influence of shear loading of the responses of strain-based elements for slender structures, a theoretically very slender cantilever beam with two different meshes was analyzed. Again, the elements such as RGR-T10, which the equilibrium conditions were applied on their assumed strain field, provided the most accurate estimations.

Finally, two problems tested the ability of the reviewed strain-based elements in the analysis of practical problems. For this purpose, two multistory single and coupled shear wall structures were analyzed to study the convergence and numerical efficiency of the strain-based formulation. The results of the single shear wall showed the fast convergence, as well, high accuracy of the strain-based element in coarse meshes compared to the classical elements. The coupled shear wall test provided a rough measure for evaluating the numerical efficiency of the studied elements by comparing the accuracy of the responses, as well as, the total number of degrees-of-freedom for two different types of meshes. It should be noted that by efficiency, the authors mean the number of elements and degrees of freedom required for a specific level of accuracy. From the numerical results in section 2, it is evident the strain-based elements provide enough accurate estimations with coarser meshes, in comparison with the classical displacement-based elements. However, to achieve a better judgment about the efficiency of the elements, the issue of computational time should also be investigated, which is not pursued in the present study and require further investigation in future research works.

4 Conclusion

Based on the performed review, many of the existing strain-based membrane elements were formulated by using linear assumed strain fields. On the other hand, most of the limited elements with higher-order strain fields were developed using incomplete higher-order polynomials, which do not provide any clear justification for the selected polynomial terms. Another interesting finding from the first part of this study was that in many of the available plane elements, the equilibrium criterion is not imposed on the assumed strain field. Moreover, it was shown that the inclusion of drilling degrees of freedom would improve the performance of resulting elements under in-plane bending. In

this part, several well-known benchmark problems were solved using the existing strain-based membrane elements and common displacement-based elements such as Q4, Q8, and LST. The obtained results clearly demonstrated the superiority of the strain-based formulation in accuracy and efficiency against displacement-based membrane elements. Various problems such as mesh sensitivity, shear, trapezoidal, and Poisson's locking were investigated, and the attained results showed that almost all the plane elements formulated by the assumed strain approach are free from these shortcomings, and even can compute response practical problems using a coarse mesh of elements. Therefore, the strain-based elements completely fit in the definition of robust finite elements. It must be added that the recently proposed higher-order triangular plane elements such as RGR-T11D-I, RGR-T11D-II, and RGR-T14 are among the best-performing elements in all the analyzed benchmark problems. This shows the merit of using higher-order assumed strain fields and imposing equilibrium equations to the opted strain components. The mentioned advantages make assumed strain formulation an interesting alternative for developing robust finite elements of different types, such as plates, shells, and solids.

Declarations

It is confirmed that the Availability of data and material, Funding, Authors' contributions, Acknowledgments, and all the subheadings of these and also the relevant information under each have been declared in this paper. Moreover, there is no conflict of interest.

References

1. Al Akhrass, D., Bruchon, J., Drapier, S. and Fayolle, S. *Integrating a logarithmic-strain based hyperelastic formulation into a three-field mixed finite element formulation to deal with incompressibility in finite-strain elastoplasticity*, Finite Elem. Anal. Des. 86 (2014) 61–70.

2. Belarbi, M.T. and Bourezane, M., *On improved Sabir triangular element with drilling rotation,* Rev. eur. génie civ., 9(9-10) (2005), 1151–1175.

3. Belarbi, M.T. and Bourezane, M. *An assumed strain based on triangular element with drilling rotation,* Courier de Savoir, 6 (2005), 117–123.

4. Belarbi, M.T. and Maalem, T. *On improved rectangular finite element for plane linear elasticity analysis,* Revue Européenne des Éléments Finis, 14(8) (2005), 985–997.

5. Cen, S., Chen, X.M. and Fu, X.R. *Quadrilateral membrane element family formulated by the quadrilateral area coordinate method*, Comput. Methods Appl. Mech. Eng. 196(41-44) (2007) 4337–4353.

6. Cen, S., Zhou, P.L., Li, C.F. and Wu, C.J. *An unsymmetric 4-node, 8-DOF plane membrane element perfectly breaking through MacNeal's theorem*, Int. J. Numer. Methods Eng. 103(7) (2015) 469–500.

7. Felippa, C.A. *A study of optimal membrane triangles with drilling freedoms,* Comput. Methods Appl. Mech. Eng. **192**(16-18) (2003), 2125–2168.

8. Hamadi, D., Ayoub, A. and Maalem, T. *A new strain-based finite element for plane elasticity problems,* Eng. Comput. 33(2) (2016), 562–579.

9. MacNeal, R.H., Harder, R.L. *A refined four-node membrane element with rotational degrees of freedom*, Comput. Struct. 28(1) (1988) 75–84.

10. Madeo, A., Casciaro, R., Zagari, G., Zinno, R. and Zucco, G. *A mixed isostatic 16 dof quadrilateral membrane element with drilling rotations, based on Airy stresses*, Finite Elem. Anal. Des. 89 (2014) 52–66.

11. Paknahad, M., Noorzaei, J., Jaafar, M.S. and Thanoon, W.A. *Analysis of shear wall structure using optimal membrane triangle element*, Finite Elem. Anal. Des. 43(11-12) (2007) 861–869.

12. Pian, T.H. and Sumihara, K. *Rational approach for assumed stress finite elements*, Int. J. Numer. Methods Eng. 20(9) (1984) 1685–1695.

13. Rebiai, C. *Finite element analysis of 2-D structures by new strain based triangular element*, J. Mech. 35(3) (2018) 1–9.

14. Rebiai, C. and Belounar, L. *A new strain based rectangular finite element with drilling rotation for linear and nonlinear analysis*, Arch. Civ. Mech. Eng. 13(1) (2013) 72–81.

15. Rebiai, C. and Belounar, L. *An effective quadrilateral membrane finite element based on the strain approach*, Measurement, 50 (2014) 263–269.

16. Rebiai, C., Saidani, N. and Bahloul, E. *A new finite element based on the strain approach for linear and dynamic analysis*, Res. J. Appl. Sci. 11(6) (2015) 639–644.

17. Rezaiee-Pajand, M., Gharaei-Moghaddam, N. and Ramezani, M. *Two triangular membrane element based on strain,* Int. J. Appl. Mech. 11(1) (2019), 1950010.

18. Rezaiee-Pajand, M., Gharaei-Moghaddam, N. and Ramezani, M.R. *A new higher-order strain-based plane element,* Scientia Iranica. Transaction A, Civil Engineering, 26(4) (2019), 2258–2275.

19. Rezaiee-Pajand, M., Gharaei-Moghaddam, N. and Ramezani, M., *Higher-order assumed strain plane element immune to mesh distortion,* Eng. Comput. 37(9) (2020), 2957–2981.

20. Rezaiee-Pajand, M., Gharaei-Moghaddam, N. and Ramezani, M., *Strain-based plane element for fracture mechanics' problems,* Theor. Appl. Fract. Mech. 108 (2020), 102569.

21. Rezaiee-Pajand, and Ramezani, M. *An evaluation of MITC and ANS elements in the nonlinear analysis of shell structures*, Mech. Adv. Mater. Struct. (2021) 1–21.

22. Rezaiee-Pajand, M., Ramezani, M. and Gharaei-Moghaddam, N. *Using higher-order strain interpolation function to improve the accuracy of structural responses,* Int. J. Appl. Mech. 12(3) (2020), 2050026.

23. Rezaiee-Pajand, M. and Yaghoobi, M. *Formulating an effective generalized four-sided element,* Eur. J. Mech. A Solids, 36 (2012), 141–155.

24. Rezaiee-Pajand, M. and Yaghoobi, M. *A free of parasitic shear strain formulation for plane element,* Research in Civil and Environmental Engineering, 1 (2013) 1–27.

25. Rezaiee-Pajand, M. and Yaghoobi, M. *A robust triangular membrane element,* Lat. Am. J. Solids Struct. 11(14) (2014), 2648–2671.

26. Rezaiee-Pajand, M. and Yaghoobi, M. *An efficient formulation for linear and geometric non-linear membrane elements,* Lat. Am. J. Solids Struct. 11(6) (2014), 1012–1035.

27. Rezaiee-Pajand, M. and Yaghoobi, M. *Two new quadrilateral elements based on strain states,* Civ. Eng. Infrastruct. J. 48(1) (2015), 133–156.

28. Sabir, A.B. *A rectangular and triangular plane elasticity element with drilling degrees of freedom,* Proceedings of the Second International Conference on Variational Methods in Engineering, Brebbia CA ed., Southampton University (1985), 17–25.

29. Sabir, A.B. and Sfendji, A. *Triangular and rectangular plane elasticity finite elements,* Thin-Walled Struct. 21(3) (1995), 225–232.

30. Tayeh, S.M. *New strain-based triangular and rectangular finite elements for plane elasticity problems,* Thesis, The Islamic University, Gaza, 2003.

31. Taylor, R.L., Beresford, P.J. and Wilson, E.L. *A non-conforming element for stress analysis*, Int. J. Numer. Methods Eng. 10(6) (1976) 1211–1219.

32. Zhang, G. and Wang, M. *Development of eight-node curved-side quadrilateral membrane element using chain direct integration scheme (SCDI) in area coordinates (MHCQ8-DI)*, Arabian Journal for Science and Engineering, 44(5) (2019) 4703–4724.